

# Ice lines as the origin for the gap/ring structure in protoplanetary disks: the issue of the assumed temperature profile

Yao Liu

Purple Mountain Observatory & Key Laboratory for Radio Astronomy, Chinese Academy of Sciences, Nanjing 210023, China; [yliu@pmo.ac.cn](mailto:yliu@pmo.ac.cn)

Received 2020 August 24; accepted 2021 February 12

**Abstract** Gaps and rings are commonly seen in recent high-resolution ALMA observations of protoplanetary disks. Ice lines of volatiles are one of the mechanisms proposed to explain the origin for these substructures. To examine the ice line hypothesis, literature studies usually parameterize the mid-plane temperature with the analytic formula of a passively heated, flared disk. The temperature in this simplified expression is basically dependent on the stellar luminosity. I have built a grid of self-consistent radiative transfer models that feature the same stellar properties, but different disk parameters. The mid-plane temperature of these models shows a large dispersion over a wide range of radii, indicating that besides the stellar luminosity, the disk parameters also play an important role in determining the thermal structure. Comparing the mid-plane temperature from radiative transfer simulation with the analytic solution shows a large difference between both approaches. This result suggests that special care on the assumed temperature profile has to be taken in the analysis of gap/ring origins, and conclusions drawn in previous works on the basis of the analytic temperature should be revisited. I further took the AS 209 disk as an example, and conducted a detailed radiative transfer modeling of the spectral energy distribution and the ALMA Band 6 image. The D137, D24 and D9 gaps are associated with the ice lines of major volatiles in the disk according to such a thorough analysis. However, if the temperature profile simply follows the analytic formula, none of these gaps matches the ice lines of the species considered here.

**Key words:** protoplanetary disks — radiative transfer — stars: formation

## 1 INTRODUCTION

Protoplanetary disks, as the birthplace of planets, have been attracting tremendous attention of study. They are a natural outcome of the star formation process, and consist of gas and dust that are the raw material for forming planets (Shu et al. 1987; Pollack et al. 1996). The properties, structure and evolution of these disks directly influence what type and the number of planets can eventually form.

The typical size of protoplanetary disks is about 100 AU (Andrews et al. 2009; Williams & Cieza 2011; Andrews et al. 2018a), corresponding to a spatial scale less than 1'' in nearby star formation regions (e.g., the distance  $D \sim 140$  pc). Therefore, high-resolution observations are required to unveil the details of the disk, especially the inner disk regions where terrestrial planets more likely form. With its unprecedented resolution and sensitivity, the Atacama Large Millimeter/submillimeter Array (ALMA)

has revealed a series of substructures in disks, among which gaps/rings are common regardless of the mass and age of the host stars (ALMA Partnership et al. 2015; Andrews et al. 2016; Long et al. 2018; Andrews et al. 2018b). In some cases, gaps/rings are not only seen in the millimeter emission but also in infrared images (e.g., van Boekel et al. 2017; Benisty et al. 2018; Avenhaus et al. 2018). The width of rings (or the depth of gaps) usually differs at different wavelengths (e.g., Huang et al. 2020; Long et al. 2020).

Planet-disk interaction is the most popular mechanism proposed to interpret the origin of the gap/ring structure (Kley & Nelson 2012). Hydrodynamic simulations of planet-disk interaction have shown that even one planet can produce multiple gaps/rings if certain conditions, for instance on the viscosity and aspect ratio of the disk, are satisfied (Dong et al. 2018). Nevertheless, applying this mechanism to real systems is very time-consuming because multifluid simulations with dust need to be run

over thousands of planetary orbits and on dense grid cells (Rosotti et al. 2016).

The gap/ring structure is also thought to be an outcome of rapid pebble growth near the condensation fronts of volatiles (Zhang et al. 2015). Volatiles freeze out onto the surface of dust grains when crossing their condensation fronts (also referred to as ice lines). Ice lines are special locations in protoplanetary disks at which a phase transition between the solid and the gaseous phase of volatile species (e.g., H<sub>2</sub>O, CO, N<sub>2</sub>) occurs. Such a phase transition induces dramatic changes in the local surface density and sticking properties of the dust grains (e.g., Birnstiel et al. 2010; Banzatti et al. 2015). Dust traps are naturally formed near the ice lines (Vericel & Gonzalez 2020), which lead to particle concentration and rapid pebble growth (Stammler et al. 2017).

Assuming a temperature profile for the disk, one can compare the location of the gaps/rings with the expected location of ice lines of major volatiles. Previous studies usually take the simplified expression for the radial temperature profile of a passively heated, flared disk in radiative equilibrium

$$T_{\text{mid}} = \left( \frac{\alpha L_{\star}}{8\pi R^2 \sigma_{\text{SB}}} \right)^{1/4}, \quad (1)$$

where  $\sigma_{\text{SB}}$  is the Stefan-Boltzmann constant, and  $L_{\star}$  is the luminosity of the central star (e.g., Chiang & Goldreich 1997; Dullemond et al. 2001). The parameter  $\alpha$  is the grazing angle at which direct stellar radiation impinges onto the disk, see figure 3 in Chiang & Goldreich (1997) for its definition. Using this analytic temperature, Long et al. (2018) and Zhang et al. (2018) found that most of the gaps and rings in their sample of disks are not associated with ice lines of major volatiles, suggesting that the ice line mechanism may not be a universal explanation for the gaps/rings.

With a given  $\alpha$ , the disk temperature described by Equation (1) is solely determined by the stellar parameters. However, as a consensus, the disk properties also have a strong impact on the thermal structure basically by altering the optical depth as functions of the radial distance and of the vertical height above the mid-plane. Furthermore, a more accurate way to calculate the temperature is to solve the radiative transfer problem with the Monte Carlo method. Therefore, it is interesting to examine how well the analytic approximation characterized by Equation (1) represents the temperature profile. Using different temperature profiles will result in different conclusions when linking the gaps/rings to ice lines. How large the difference would be is also desired to be investigated.

In this work, I build self-consistent radiative transfer models, with stellar parameters fixed and disk parameters

**Table 1** Parameter Sampling of the Model Grid

Parameter	Value	Number
$M_{\star} [M_{\odot}]$	0.5	1
$T_{\star} [\text{K}]$	4000	1
$L_{\star} [L_{\odot}]$	0.92	1
$R_{\text{in}} [\text{AU}]$	0.1	1
$R_{\text{c}} [\text{AU}]$	100	1
$\Lambda$	0.2	1
$f$	0.95	1
$\gamma$	0.5, 1.0, 1.5	3
$\beta$	1.05, 1.10, 1.15, 1.20, 1.25	5
$h_{\text{c}} [\text{AU}]$	5, 10, 15, 20	4
$M_{\text{dust}} [M_{\odot}]$	$5 \times 10^{-6}$ , $5 \times 10^{-5}$ , $5 \times 10^{-4}$	3

varying within reasonable ranges (Sect. 2). Then, I discuss the difference in the mid-plane temperature between the models and the one predicted by the analytic formula (Sect. 3). In Section 4, as an illustration, I conduct a detailed modeling of the AS 209 disk, and show the implication of using different temperature profiles on the analysis of gaps/rings origin. The paper ends up with a brief summary in Section 5.

## 2 PARAMETRIC RADIATIVE TRANSFER MODELS

In this section, I first describe the assumption and setup of the radiative transfer model, and then create a grid of models by sampling a few key parameters that are expected to affect the temperature structure.

### 2.1 Model Description

#### 2.1.1 Dust density structure

I employ a flared disk model that includes two distinct dust grain populations, i.e., a small grain population (SGP) and a large grain population (LGP). The inner radius and total dust mass of the disk are denoted as  $R_{\text{in}}$  and  $M_{\text{dust}}$ , respectively.

The SGP occupies a minor fraction of the dust mass,  $(1 - f) M_{\text{dust}}$ , and is distributed vertically following a power-law profile:

$$h = h_{\text{c}} \times \left( \frac{R}{R_{\text{c}}} \right)^{\beta}. \quad (2)$$

The flaring index is quantified with  $\beta$ , and  $h_{\text{c}}$  refers to the scale height at a fixed characteristic radius  $R_{\text{c}}$ . Conversely, the LGP dominates the dust mass,  $f M_{\text{dust}}$ , and is concentrated close to the mid-plane with a scale height  $\Lambda h$ , where the parameter  $\Lambda < 1$ . Such a two-layer disk model is a common prescription used to account for the effect of dust settling in protoplanetary disks (e.g., Dullemond & Dominik 2004; D’Alessio et al. 2006; Andrews et al. 2011; Liu et al. 2019). The surface density

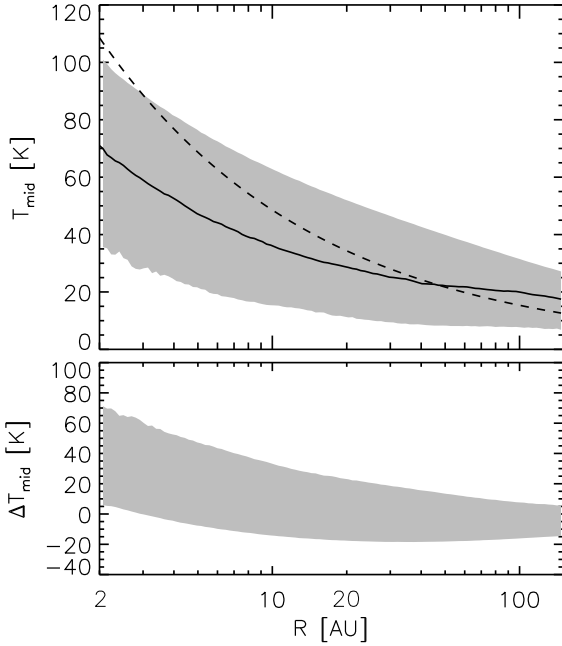


**Fig. 1** *Upper panel:* the shaded area gives the range of the mid-plane temperature ( $T_{\text{RT}}$ ) extracted from the 180 radiative transfer models. The solid line refers to the median level of  $T_{\text{RT}}$ . The analytic temperature profile ( $T_{\text{ana}}$ ) is indicated with the dashed line. *Lower panel:* the difference ( $\Delta T = T_{\text{ana}} - T_{\text{RT}}$ ) between  $T_{\text{ana}}$  and  $T_{\text{RT}}$  are shown as the shaded region.

profile is taken as a power law with an exponential taper

$$\Sigma \propto \left(\frac{R}{R_c}\right)^{-\gamma} \exp\left[-\left(\frac{R}{R_c}\right)^{2-\gamma}\right], \quad (3)$$

where  $\gamma$  is the gradient parameter. This is the similarity solution for disk evolution, which assumes that the viscosity has a power-law radial dependence and is independent of time (Lynden-Bell & Pringle 1974). The volume density of the dust grains is parameterized as

$$\rho_{\text{SGP}} \propto \frac{(1-f)\Sigma}{h} \exp\left[-\frac{1}{2}\left(\frac{z}{h}\right)^2\right], \quad (4)$$

$$\rho_{\text{LGP}} \propto \frac{f\Sigma}{\Lambda h} \exp\left[-\frac{1}{2}\left(\frac{z}{\Lambda h}\right)^2\right]. \quad (5)$$

The proportionality factors of Equations (3), (4) and (5) are determined by normalizing the total dust mass in the disk.

### 2.1.2 Dust properties

The dust ensemble consists of astronomical silicate and graphite, with relative abundances of 62.5% for silicate and 37.5% for graphite. The refractive indices of “smoothed astronomical silicate” and graphite are taken from Weingartner & Draine (2001). I use the Mie theory to calculate the mass absorption/scattering coefficients. The

grain size distribution follows the power law  $dn(a) \propto a^{-3.5}da$  with a minimum grain size fixed to  $a_{\text{min}} = 0.01 \mu\text{m}$ . The maximum grain size is set to  $a_{\text{max}} = 2 \mu\text{m}$  for the SGP and  $a_{\text{max}} = 3 \text{mm}$  for the LGP, respectively.

### 2.1.3 Heating mechanisms

Stellar irradiation and viscous accretion are the major heating sources in protoplanetary disks. In the simulation, only stellar heating is taken into account. The effect of viscous heating is discussed in Section 3.2. To mimic a T Tauri star, I assume a stellar luminosity  $L_\star = 0.92 L_\odot$ , stellar mass  $M_\star = 0.5 M_\odot$  and an effective temperature  $T_{\text{eff}} = 4000 \text{K}$  (Gullbring et al. 1998). The stellar spectrum is taken from the Kurucz (1994) database, assuming  $\log g = 3.5$  and solar metallicity.

## 2.2 Establishment of the Model Grid

Table 1 summarizes the parameters of the model. The flaring index ( $\beta$ ) and scale height ( $h_c$ ) work together to determine the disk geometry, therefore to alter the grazing angle ( $\alpha$ ). The larger  $\alpha$  is, the more stellar energy absorbed by the disk would be, which in turn results in a higher temperature. With the dust model assumed in Section 2.1.2, the total dust mass ( $M_{\text{dust}}$ ) and the gradient parameter ( $\gamma$ ) for the surface density set up the optical depth of the disk as a function of radius ( $R$ ), and therefore affect the scale height above which the photons from the central star are absorbed. Consequently, both  $M_{\text{dust}}$  and  $\gamma$  have an impact on the disk temperature profile.

The main goal of this work is to investigate the mid-plane temperature of radiative transfer models with different disk parameters. Hence, I build a model grid, in which  $\beta$ ,  $h_c$ ,  $M_{\text{dust}}$  and  $\gamma$  are explored. Specifically,  $\beta$ ,  $h_c$ , and  $\gamma$  are sampled in reasonable ranges that are consistent with results derived from modelling multiwavelength observations of protoplanetary disks (e.g., Andrews et al. 2009, 2011; Kirchschlager et al. 2016; Liu et al. 2019). The total dust mass varies in a range of  $[5 \times 10^{-6}, 5 \times 10^{-4} M_\odot]$  that is typically derived from millimeter observations (e.g., Andrews et al. 2013; Pascucci et al. 2016). Since the stellar mass is fixed to  $0.5 M_\odot$ , the disk mass (dust + gas) to stellar mass ratio  $M_{\text{D}}/M_\star$  lies in a range of  $[0.001, 0.1]$ , assuming a standard gas-to-dust mass ratio of 100.

The grid points in each dimension are tabulated in Table 1. There are 180 models in total. To solve the problem of continuum radiative transfer, I employ the RADMC-3D<sup>1</sup> package (Dullemond et al. 2012), and use  $10^8$  photons in the Monte Carlo simulation because these

<sup>1</sup> <http://www.ita.uni-heidelberg.de/~dullemond/software/radmc-3d/>.

many photons are necessary to achieve a low level of noise in the mid-plane temperature.

### 3 RESULT AND DISCUSSION

#### 3.1 The Mid-plane Temperature Profile

The mid-plane temperatures ( $T_{\text{RT}}$ ) of the 180 radiative transfer models are shown as the shaded area in the upper panel of Figure 1. The solid line refers to the median temperature of these models. As can be seen, even though the stellar properties are fixed, the temperature shows a large dispersion among models with different disk parameters. The dispersion is around 60 K in the inner disk regions ( $R \lesssim 10$  AU), and decreases to  $\sim 20$  K at  $R = 100$  AU. The analytic expression ( $T_{\text{ana}}$ ) is indicated with the dashed line. The grazing angle  $\alpha$  was set to 0.05, a typical value for protoplanetary disks and commonly adopted in literature studies (Dullemond & Dominik 2004). It is clear that the distribution of  $T_{\text{RT}}$  is shallower than that of  $T_{\text{ana}}$ , and  $T_{\text{RT}}$  is generally lower than  $T_{\text{ana}}$  in the inner disk.

The lower panel of Figure 1 shows the difference  $\Delta T = T_{\text{ana}} - T_{\text{RT}}$  between both methods, with  $\Delta T$  ranging from  $-20$  K to  $+60$  K. Therefore, the analytic solution is not a good approximation for the mid-plane temperature profile. The condensation temperatures of  $\text{N}_2$ , CO, and clathrate-hydrated CO and  $\text{N}_2$ , as some of the major volatiles in protoplanetary disks, are 12–15 K, 23–28 K, and 41–46 K, respectively, which are calculated under realistic pressure ranges in the disk mid-plane (Zhang et al. 2015). The difference ( $\Delta T$ ) between  $T_{\text{ana}}$  and  $T_{\text{RT}}$  is comparable with (even larger than) these condensation temperatures. Consequently, using the analytic formula in the analysis of gaps/rings origin will lead to incorrect association (or mismatch) between the gap/ring location and condensation fronts of volatiles.

#### 3.2 The Effect of Viscous Heating

As laid out in Section 2.1.3, the disk is passively heated by stellar irradiation. Figure 2 illustrates the effect of viscous heating on the temperature distribution. The solid line shows one model in the grid calculated in Section 2.2. Model parameters are  $\gamma = 1.0$ ,  $\beta = 1.15$ ,  $h_c = 10$  AU, and  $M_{\text{dust}} = 5 \times 10^{-5} M_{\odot}$ . The dashed line is the same model, but viscous heating is included as well. To do this, the dissipated energy per unit area generated by viscosity is assumed as

$$\dot{E} = \frac{3GM_{\star}\dot{M}_{\text{acc}}}{8\pi R^3} \left[ 1 - \left( \frac{R_{\star}}{R} \right)^{1/2} \right], \quad (6)$$

where  $G$  is the gravitational constant (Hartmann 2009). The accretion rate is chosen to be  $\dot{M}_{\text{acc}} = 10^{-8} M_{\odot} \text{ yr}^{-1}$

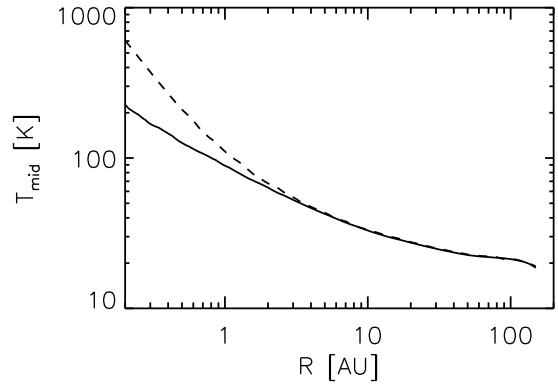


**Fig. 2** Comparison of the mid-plane temperature between models that consider different heating mechanisms. The solid line refers to a model in which only stellar irradiation is taken into account, whereas the dashed line shows the same model that includes both viscous heating and stellar irradiation.

that is typical for T Tauri stars (e.g., Hartmann et al. 1998; Manara et al. 2016). The photon packages carrying the dissipated energy originates directly from the disk mid-plane in the simulation.

As can be seen in Figure 2, viscous accretion does not have a significant impact on the temperature for most regions in the disk ( $R \gtrsim 2$  AU). This conclusion is consistent with findings by previous works, in which viscous heating is added via different approaches (e.g., Garaud & Lin 2007; Harsono et al. 2015).

### 4 APPLICATION TO AS 209

Based on a grid of radiative transfer models, I have found that the analytic formula, commonly used in the analysis of gap origins, cannot describe the mid-plane temperature profile of the disk well. Moreover, besides stellar properties, the temperature is highly dependent on the disk properties that can be constrained through detailed modelling of multiwavelength observations. In this section, I take the AS 209 disk as an example, and examine whether the gaps are correlated with condensation fronts of volatiles.

AS 209, also known as V1121 Oph, is a classical T Tauri star (spectral type K4) located in the  $\rho$ -Ophiuchus cloud at a distance of  $D = 121$  pc (Torres et al. 2006; Gaia Collaboration et al. 2018). The disk around AS 209 presents a series of concentric gaps and rings as unveiled by the recent ALMA Band 6 ( $\lambda \sim 1.25$  mm) observation with an unprecedented angular resolution  $0.038'' \times 0.036''$  (Andrews et al. 2018b), see the left panel of Figure 3. The azimuthally-averaged surface brightness of the 1.25 mm dust continuum is indicated with the red dots in the left panel of Figure 4, in which the locations and names of gaps identified by Huang et al. (2018) are marked

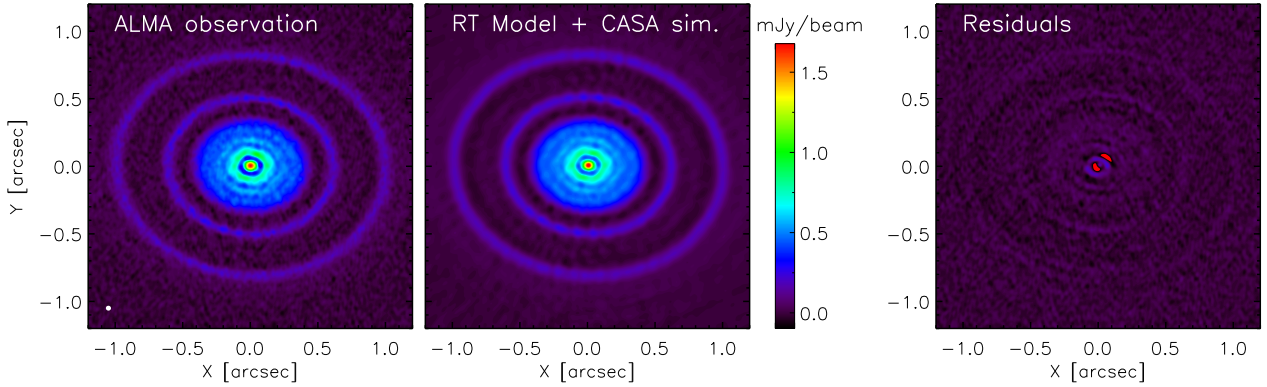


**Fig. 3** Comparison between the ALMA observation (*left*) and the model image (*middle*) at 1.25 mm for the AS 209 disk. The tiny beam ( $0.038'' \times 0.036''$ ) is indicated with the white-filled ellipse in the lower left corner of the observed image. The *right* panel shows the residuals between the observed and model maps.

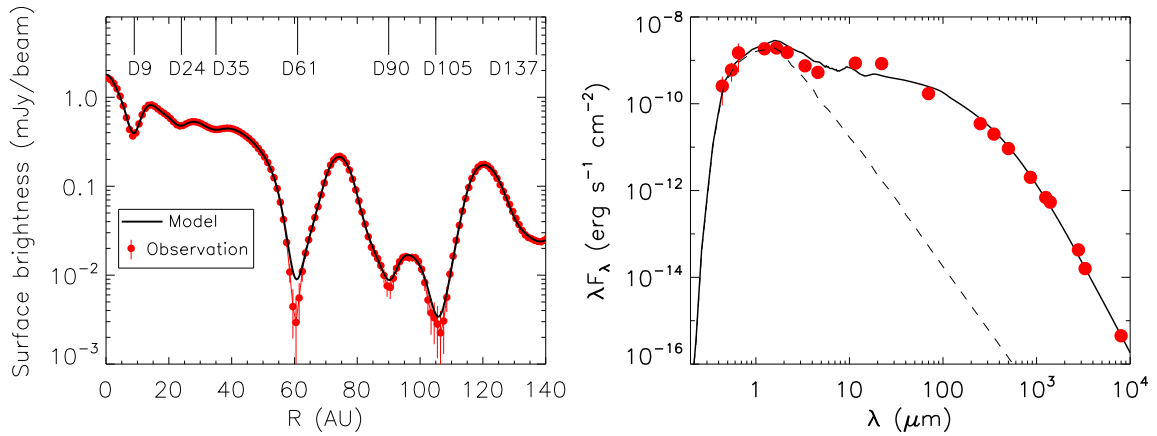


**Fig. 4** *Left panel*: comparison of the azimuthally-averaged surface brightness between model and observation. *Right panel*: the SED of the AS 209 disk. The solid line shows the model prediction, whereas the dashed curve indicates the photospheric emission level. Red dots are the data points measured at various wavelengths from optical (Grankin et al. 2007), to infrared (Cutri et al. 2003; Cutri & et al. 2014; Marton et al. 2016), and to millimeter (Andrews et al. 2009; Ricci et al. 2010; Pérez et al. 2012; Huang et al. 2016; Andrews et al. 2018b)

as well. Through hydrodynamical simulations of planet-disk interaction, Zhang et al. (2018) found that one planet located at  $R \sim 99$  AU can produce the gap around 100 AU, and is also able to match the positions of the D61, D35, and even the D24 gaps. The mass of the putative planet is  $0.087 M_J$ , where  $M_J$  is the mass of Jupiter.

In order to investigate the condensation fronts as the origin for the gap/ring structure, I conduct a detailed radiative transfer modeling of the spectral energy distribution (SED) and the 1.25 mm dust continuum image. The modeling procedure consists of three steps. First, given the stellar parameters of AS 209, a grid of model SEDs is established. The assumed density structure and dust properties are identical to those described in Section 2.1. The purpose of this step is to constrain the geometry parameters (i.e.,  $\beta$  and  $h_c$ ) of the disk by fitting the SED alone. The second step is to build the surface density profile of the LGP. The task requires an iterative process

that fits the azimuthally-averaged surface brightness of the 1.25 mm dust continuum. Details about this approach can be found in Liu et al. (2019). The constructed surface density of the LGP goes into the last step, which fits the SED and the 1.25 mm image simultaneously using the Markov Chain Monte Carlo method.

The best-fit model is presented in Figures 3 and 4. To simulate an ALMA observation of the best-fit model, I compute the model visibilities at the exactly same uv coordinates of the observation. Using the Common Astronomy Software Applications (CASA) package (McMullin et al. 2007), the resulting data set of model visibilities was CLEANed with the same parameters as for the observation<sup>2</sup>.

The mid-plane temperature of the best-fit model is shown as the solid line in Figure 5. The effects of each individual parameter on the temperature are investigated,

<sup>2</sup> <https://almascience.org/alma-data/lp/DSHARP>

with results presented in Section A. The profile shows two bumps in the D61, D90, and D105 gap region. This is presumably due to an enhanced irradiation of thermal emission from the neighbouring rings. The shaded areas denote the range of condensation temperature for  $N_2$  (cyan), CO (grey) and clathrate-hydrated CO and  $N_2$  (green), respectively. The plot indicates that the D137, D24 and D9 gaps are associated with the condensation fronts of these species. However, none of these gaps is likely produced via the ice lines of the volatiles considered here, if the temperature follows the analytic solution, see the dashed line in Figure 5.

## 5 SUMMARY

Recent high angular resolution observations with ALMA have demonstrated that gaps and rings are prevalent substructures in protoplanetary disks. Various theories were proposed to interpret the formation of gaps and rings. One of the popular mechanisms is due to rapid pebble growth near the ice lines of volatiles. To examine this hypothesis in real systems, one needs to compare the location of the observed gaps/rings with the expected location of ice lines of major volatiles. Such a comparison requires an assumption for the temperature profile of the disk mid-plane. Previous works usually adopt the analytic expression for an irradiated flared disk, which is mainly governed by the stellar luminosity. It is poorly known how well the analytic approximation is.

Radiative transfer modeling is a more accurate way to calculate the thermal structure of disks. By sampling the disk parameters within reasonable ranges, I have built a grid of radiative transfer models with the same stellar parameters. The mid-plane temperature of these models shows a large dispersion over a wide range of radii, indicating the important role of disk properties in determining the temperature structure. Moreover, there are obvious discrepancies in the temperature between the models and the analytic prediction.

I further took the AS 209 disk as an example to show the implication of using different temperature profiles in the analysis of gaps/rings origin. I built a self-consistent radiative transfer model of the AS 209 disk, which can simultaneously fit the SED and the high-resolution ALMA image. Such a detailed analysis shows that the D137, D24 and D9 gaps are associated with the ice lines of major volatiles in the disk. However, the ice line mechanism is not able to explain any of these gaps if the simplified analytic temperature profile is assumed. Therefore, conclusions drawn in the literature on the basis of the analytic temperature need to be revisited, and multiwavelength radiative transfer modeling is a preferable

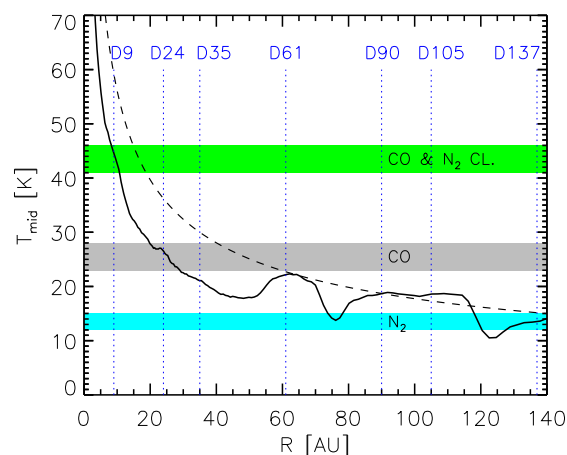


**Fig. 5** The expected condensation fronts in the mid-plane of the AS 209 disk. The condensation temperature ranges for  $N_2$  (cyan), CO (grey) and clathrate-hydrated CO and  $N_2$  (green) are indicated with shaded areas. The solid line refers to the mid-plane temperature of the best-fit radiative transfer model, while the analytic profile is shown as the dashed line. The vertical dotted lines mark the location of the gaps. The nomenclature for the gap is the same as introduced by Huang et al. (2018).

means to investigate the ice line mechanism as the origin for gaps and rings.

**Acknowledgements** YL acknowledges financial support by the Natural Science Foundation of Jiangsu Province of China (Grant No. BK20181513) and by the National Natural Science Foundation of China (Grant No. 11973090). YL thanks Ewine F. van Dishoeck and Fujun Du for insightful discussions. *Herschel* is an ESA space observatory with science instruments provided by European-led Principal Investigator consortia and with important participation from NASA. ALMA is a partnership of ESO (representing its member states), NSF (USA), and NINS (Japan), together with NRC (Canada), MOST and ASIAA (Taiwan, China), and KASI (Republic of Korea), in cooperation with the Republic of Chile. The Joint ALMA Observatory is operated by ESO, AUI/NRAO, and NAOJ.

## Appendix A: THE EFFECTS OF DISK PARAMETERS ON THE MID-PLANE TEMPERATURE

In this section, the effect of each disk parameter on the temperature profile is investigated. The explored parameters are the flaring index  $\beta$ , scale height  $h_c$ , the power-law index of the surface density  $\gamma$ , and dust mass  $M_{\text{dust}}$ . The results are presented in Figure A.1. The best-fit model of the AS 209 disk is indicated as the black solid line in each panel. The corresponding parameters are  $\beta = 1.1$ ,

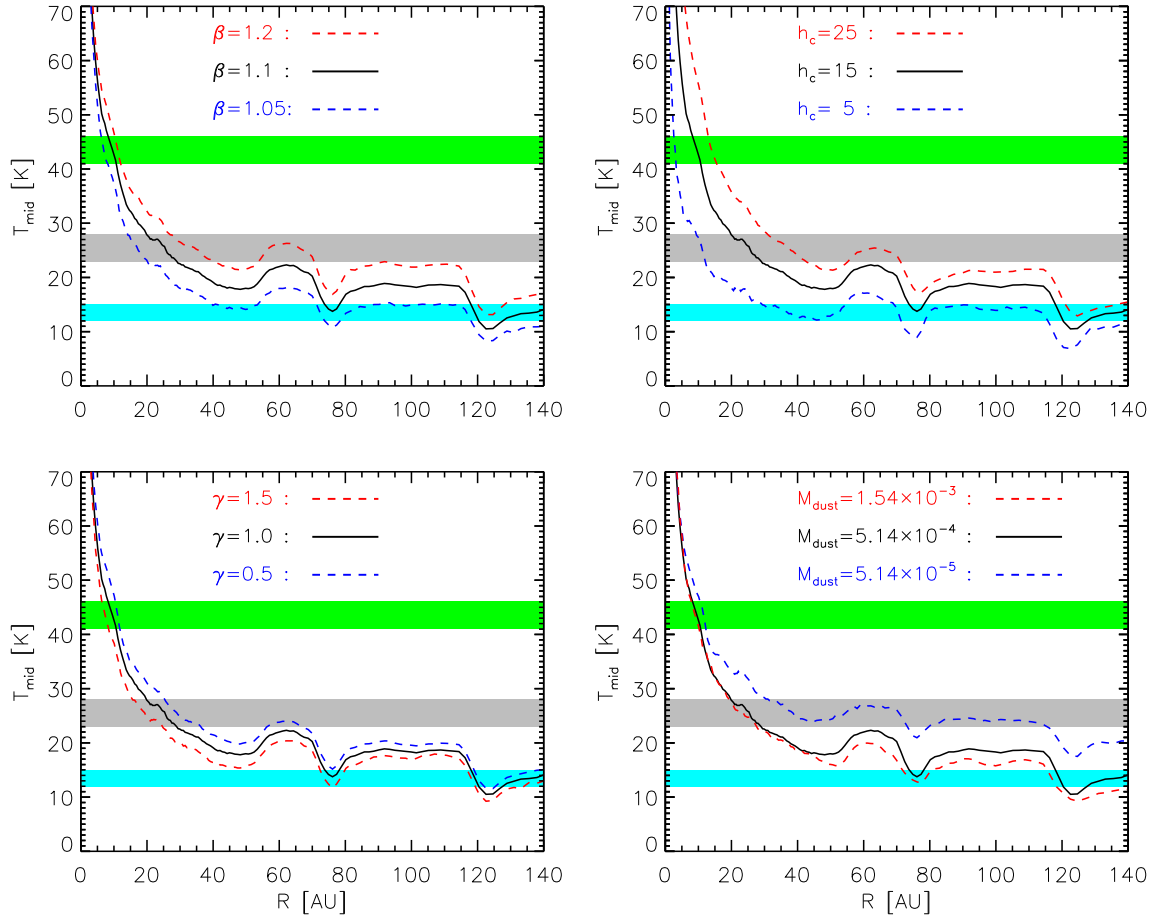


**Fig. A.1** The effect of disk parameters on the mid-plane temperature. The condensation temperature ranges for N<sub>2</sub> (cyan), CO (grey) and clathrate-hydrated CO and N<sub>2</sub> (green) are indicated with shaded areas.

$h_c = 15$  AU,  $\gamma = 1.0$  and  $M_{\text{dust}} = 5.14 \times 10^{-4} M_{\odot}$ . More flared disks or disks featuring larger scale heights intercept more stellar energy, leading to an overall higher temperature. The total dust mass and power-law index of the surface density combine to determine the optical depth. In disks with higher optical depth, stellar photons are absorbed at higher altitudes, and therefore the dense mid-plane becomes cooler.

## References

- ALMA Partnership, Brogan, C. L., Pérez, L. M., et al. 2015, *ApJL*, 808, L3
- Andrews, S. M., Rosenfeld, K. A., Kraus, A. L., & Wilner, D. J. 2013, *ApJ*, 771, 129
- Andrews, S. M., Terrell, M., Tripathi, A., et al. 2018a, *ApJ*, 865, 157
- Andrews, S. M., Wilner, D. J., Espaillat, C., et al. 2011, *ApJ*, 732, 42
- Andrews, S. M., Wilner, D. J., Hughes, A. M., Qi, C., & Dullemond, C. P. 2009, *ApJ*, 700, 1502
- Andrews, S. M., Wilner, D. J., Zhu, Z., et al. 2016, *ApJL*, 820, L40
- Andrews, S. M., Huang, J., Pérez, L. M., et al. 2018b, *ApJL*, 869, L41
- Avenhaus, H., Quanz, S. P., Garufi, A., et al. 2018, *ApJ*, 863, 44
- Banzatti, A., Pinilla, P., Ricci, L., et al. 2015, *ApJL*, 815, L15
- Benisty, M., Juhász, A., Facchini, S., et al. 2018, *A&A*, 619, A171
- Birnstiel, T., Dullemond, C. P., & Brauer, F. 2010, *A&A*, 513, A79
- Chiang, E. I., & Goldreich, P. 1997, *ApJ*, 490, 368
- Cutri, R. M., & et al. 2014, *VizieR Online Data Catalog*, II/328
- Cutri, R. M., Skrutskie, M. F., van Dyk, S., et al. 2003, *VizieR Online Data Catalog*, II/246
- D’Alessio, P., Calvet, N., Hartmann, L., Franco-Hernández, R., & Servín, H. 2006, *ApJ*, 638, 314
- Dong, R., Li, S., Chiang, E., & Li, H. 2018, *ApJ*, 866, 110
- Dullemond, C. P., & Dominik, C. 2004, *A&A*, 421, 1075
- Dullemond, C. P., Dominik, C., & Natta, A. 2001, *ApJ*, 560, 957
- Dullemond, C. P., Juhász, A., Pohl, A., et al. 2012, *RADMC-3D: A Multi-purpose Radiative Transfer Tool*, *Astrophysics Source Code Library*, ascl:1202.015

- Gaia Collaboration, Brown, A. G. A., Vallenari, A., et al. 2018, *A&A*, 616, A1
- Garaud, P., & Lin, D. N. C. 2007, *ApJ*, 654, 606
- Grankin, K. N., Melnikov, S. Y., Bouvier, J., Herbst, W., & Shevchenko, V. S. 2007, *A&A*, 461, 183
- Gullbring, E., Hartmann, L., Briceño, C., & Calvet, N. 1998, *ApJ*, 492, 323
- Harsono, D., Bruderer, S., & van Dishoeck, E. F. 2015, *A&A*, 582, A41
- Hartmann, L. 2009, *Accretion Processes in Star Formation: Second Edition* (UK: Cambridge Univ. Press)
- Hartmann, L., Calvet, N., Gullbring, E., & D'Alessio, P. 1998, *ApJ*, 495, 385
- Huang, J., Öberg, K. I., & Andrews, S. M. 2016, *ApJL*, 823, L18
- Huang, J., Andrews, S. M., Dullemond, C. P., et al. 2018, *ApJL*, 869, L42
- Huang, J., Andrews, S. M., Dullemond, C. P., et al. 2020, *ApJ*, 891, 48
- Kirchschlager, F., Wolf, S., & Madlener, D. 2016, *MNRAS*, 462, 858
- Kley, W., & Nelson, R. P. 2012, *ARA&A*, 50, 211
- Kurucz, R. 1994, *Solar Abundance Model Atmospheres for 0,1,2,4,8 km/s* (Kurucz CD-ROM No. 19. Cambridge), Mass: Smithsonian Astrophysical Observatory, 1994, 19
- Liu, Y., Dipierro, G., Ragusa, E., et al. 2019, *A&A*, 622, A75
- Long, F., Pinilla, P., Herczeg, G. J., et al. 2018, *ApJ*, 869, 17
- Long, F., Pinilla, P., Herczeg, G. J., et al. 2020, *ApJ*, 898, 36
- Lynden-Bell, D., & Pringle, J. E. 1974, *MNRAS*, 168, 603
- Manara, C. F., Fedele, D., Herczeg, G. J., & Teixeira, P. S. 2016, *A&A*, 585, A136
- Maron, G., Schulz, B., Altieri, B., et al. 2016, in *IAU Symposium*, 315, *From Interstellar Clouds to Star-Forming Galaxies: Universal Processes?* eds. P. Jablonka, P. André, & F. van der Tak, E53
- McMullin, J. P., Waters, B., Schiebel, D., Young, W., & Golap, K. 2007, in *Astronomical Society of the Pacific Conference Series*, 376, *Astronomical Data Analysis Software and Systems XVI*, eds. R. A. Shaw, F. Hill, & D. J. Bell, 127
- Pascucci, I., Testi, L., Herczeg, G. J., et al. 2016, *ApJ*, 831, 125
- Pérez, L. M., Carpenter, J. M., Chandler, C. J., et al. 2012, *ApJL*, 760, L17
- Pollack, J. B., Hubickyj, O., Bodenheimer, P., et al. 1996, *Icarus*, 124, 62
- Ricci, L., Testi, L., Natta, A., & Brooks, K. J. 2010, *A&A*, 521, A66
- Rosotti, G. P., Juhasz, A., Booth, R. A., & Clarke, C. J. 2016, *MNRAS*, 459, 2790
- Shu, F. H., Adams, F. C., & Lizano, S. 1987, *ARA&A*, 25, 23
- Stammler, S. M., Birnstiel, T., Panić, O., Dullemond, C. P., & Dominik, C. 2017, *A&A*, 600, A140
- Torres, C. A. O., Quast, G. R., da Silva, L., et al. 2006, *A&A*, 460, 695
- van Boekel, R., Henning, T., Menu, J., et al. 2017, *ApJ*, 837, 132
- Vericel, A., & Gonzalez, J.-F. 2020, *MNRAS*, 492, 210
- Weingartner, J. C., & Draine, B. T. 2001, *ApJ*, 548, 296
- Williams, J. P., & Cieza, L. A. 2011, *ARA&A*, 49, 67
- Zhang, K., Blake, G. A., & Bergin, E. A. 2015, *ApJL*, 806, L7
- Zhang, S., Zhu, Z., Huang, J., et al. 2018, *ApJL*, 869, L47